

Scanning total internal reflection fluorescence microscopy and its applications

James W. M. Chon* and Min Gu
Centre for Micro-Photonics,
School of Biophysical Sciences and Electrical Engineering,
Swinburne University of Technology,
P. O. Box 218, Hawthorn, 3122, Australia

ABSTRACT

In this paper, we explore the multiphoton excitation capabilities of the scanning total internal reflection fluorescence microscopy (STIRFM) using a focused ring-beam illumination and a high numerical-aperture objective (NA = 1.65). The evanescent field produced by the STIRFM is focused laterally, producing a small excitation volume that can effectively induce non-linear optical process. The theoretical simulation of the focal spot produced in STIRFM geometry shows that the focused evanescent field is split into two peaks due to the strong enhancement of longitudinal polarization component at the focus of a high numerical-aperture objective. Experimental images of two-photon excited CdSe quantum dot nanocrystals show the characteristic split focal spot.

1. INTRODUCTION

Due to the ability of strong attenuation of the background fluorescence, total internal reflection fluorescence microscopy (TIRFM) has been the major technique in the fluorescence imaging and single molecule detections. At present, there are two geometries of TIRFM, the prism-type [1-6, 8-12] and the objective-type [5-7]. In a prism-type TIRFM, an evanescent field is generated by directing a laser beam at an angle larger than the critical angle at the interface between the prism and a sample. In an objective-type TIRFM, a beam is directed to a small portion of the entrance pupil of high numerical aperture objective to meet the TIR condition. Both geometries require cumbersome experimental procedures that are difficult to implement.

Recently, a new type of TIRFM called scanning TIRFM (henceforth abbreviated STIRFM) was proposed. The STIRFM employs localized evanescent field as a sensing probe. The tight confinement of evanescent field is achieved by focusing the ring-beam illumination at the interface with high numerical aperture objective, and it is shown to improve both transverse and axial resolution. The enhancement of the longitudinal polarization at the evanescent focus is also proved useful in fluorescence polarization microscopy. Furthermore, with a highly focused beam, it is predicted to induce a non-linear effect such as two-photon absorption at the focus, although yet to be verified.

In this paper, we explore the multiphoton excitation capability of STIRFM. The ability to confine evanescent field and induce non-linear optical process will be useful in near-field imaging and near-field data storage applications

*Email: jchon@swin.edu.au; Phone: 61-3-92144326; Fax: 61-3-92145435

such as super-resolution near-field structure (super-Rens) [18]. In Section 2, theoretical simulations of the evanescent focal shape produced by the STIRFM are presented, for one-photon and two-photon excitation. In Section 3, we present the experimental setup and the imaging results of STIRFM, to verify the non-linear optical imaging capabilities of the current setup. In particular, we present the images of CdSe quantum dots to characterize imaging resolution, and the evanescent focal shape of STIRFM. Finally we give conclusions in Section 4.

2. THEORETICAL SIMULATION OF FOCUS PRODUCED BY STIRFM

2.1 Illumination point spread function

In STIRFM, focusing with a high numerical-aperture objective induces the depolarization of the input beam. In order to account for the depolarization effect in simulating the focus produced by STIRFM, the vectorial Debye theory is employed [15, 16]. When a linearly polarized coherent monochromatic plane light wave is focused through an index-mismatched interface by a high numerical-aperture objective, the electric field in the focal region of the objective can be expressed as

$$\mathbf{E}(r_2, \phi, z_2) = \frac{\pi i}{\lambda} \{ [I_0 + \cos(2\phi)I_2] \mathbf{i} + \sin(2\phi)I_2 \mathbf{j} + 2i \cos\phi I_1 \mathbf{k} \}. \quad (1)$$

where \mathbf{i} , \mathbf{j} , and \mathbf{k} are the unit vectors in the x , y , and z directions, respectively. The incident polarization is assumed in the x – direction. It is clear that \mathbf{E} is depolarized and has three components E_x , E_y , and E_z . Variables r_2 , ϕ and z_2 are the cylindrical coordinates of an observation point. Here the definition of three variables I_0 , I_1 and I_2 is given by

$$I_0 = \int_{\beta}^{\alpha} \sqrt{\cos\theta_1} \sin\theta_1 (t_s + t_p \cos\theta_2) \exp[-ik_0 \Phi(\theta_1)] J_0(k_1 r_2 \sin\theta_1) \exp(-ik_2 z_2 \cos\theta_2) d\theta_1 \quad (2)$$

$$I_1 = \int_{\beta}^{\alpha} \sqrt{\cos\theta_1} \sin\theta_1 (t_p \sin\theta_2) \exp[-ik_0 \Phi(\theta_1)] J_1(k_1 r_2 \sin\theta_1) \exp(-ik_2 z_2 \cos\theta_2) d\theta_1 \quad (3)$$

$$I_2 = \int_{\beta}^{\alpha} \sqrt{\cos\theta_1} \sin\theta_1 (t_s - t_p \cos\theta_2) \exp[-ik_0 \Phi(\theta_1)] J_2(k_1 r_2 \sin\theta_1) \exp(-ik_2 z_2 \cos\theta_2) d\theta_1 \quad (4)$$

Where $J_0(x)$, $J_1(x)$ and $J_2(x)$ are the zero-order, the first-order and the second-order Bessel functions of the first kind, α and β are the convergence angles of waves corresponding to the outer and inner radii of a ring beam, respectively, and the aberration correction function $\Phi(\theta_1)$ is given by

$$\Phi(\theta_1) = -d(n_1 \cos\theta_1 - n_2 \cos\theta_2), \quad (5)$$

where d is the distance between the interface and the focal point of the objective. The intensity is proportional to the modulus squared of Eq. (1).

Fig. 1 gives the contour plots ($v_x = kx \sin\alpha$ and $v_y = ky \sin\alpha$) of the normalized intensity $|\mathbf{E}|^2$ and its components $|E_x|^2$, $|E_y|^2$ and $|E_z|^2$ in the x , y , and z directions near the focal region at the coverslip glass ($n=1.78$) and air interface ($d=0$), when an objective of NA=1.65 is illuminated by a ring beam ($\epsilon_{outer} = 1$, i.e. $\alpha = 68^\circ$ and $\epsilon_{inner} = \epsilon_c$, i.e. $\beta = 35^\circ$). Because the inner radius of the ring beam is calculated to be equal to the critical radius (ϵ_c), the produced focus is evanescent in nature. As expected, because of the factors $\cos(2\phi)$, $\sin(2\phi)$, and $\cos(\phi)$ in

Eq. (1) and the relative strength of Bessel functions, $J_0(x)$, $J_1(x)$ and $J_2(x)$, the patterns of $|E_x|^2$, $|E_y|^2$ and $|E_z|^2$ exhibit one, four and two lobes, respectively. The splitting of the focus in the direction of polarization (x -direction) is visibly clear in the $|E|^2$ distribution (Fig. 1d) and it is induced by the contribution from $|E_z|^2$. In a similar fashion to the free-space splitting, the relative strength or the weighting of $|E_z|^2$ to $|E_x|^2$ component governs the overall shape of the focus [13].

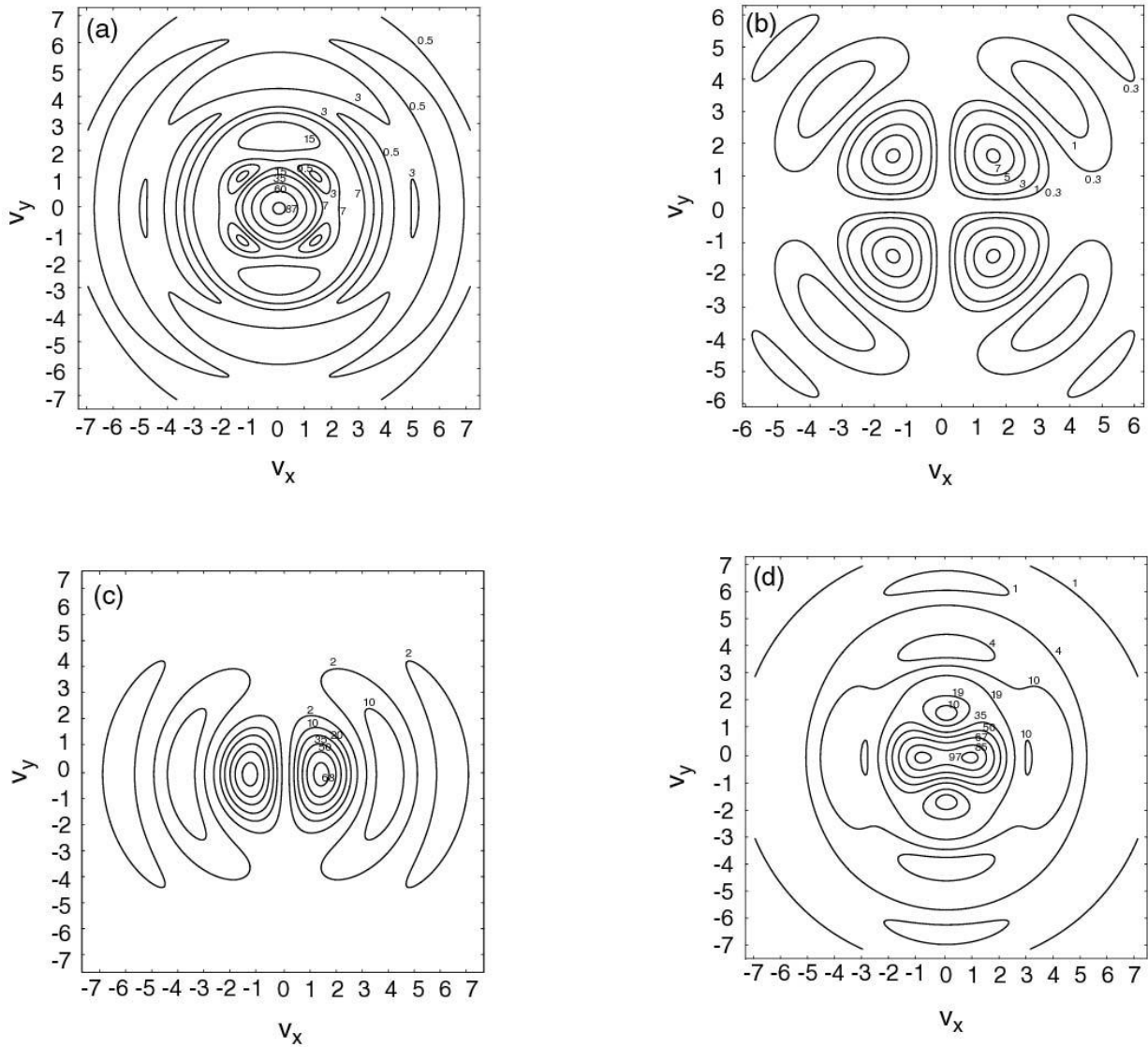


FIGURE 1: Contour plots of intensity near the focus of an objective illuminated by a ring beam ($\epsilon=0.6$). (a) $|E_x|^2$, (b) $|E_y|^2$, (c) $|E_z|^2$, (d) $|E|^2$. Peak intensities of $|E|^2$ has been normalized to 100 and the incident polarization is in parallel with the x -axis. The numerical aperture is assumed to be 1.65.

2.2 One-photon and two-photon image formation in STIRFM

In the previous section, the theoretical studies predicts of focus-splitting in STIRFM. For one-photon excitation, it is customary to put a pinhole in front of the detection system to reduce the background scattered signal. Consequently, the detection path is confocal in nature and the effective point spread function (denoted by H) in this case is given by [17],

$$H_{1p} = h_{ill}h_{det}, \quad (6)$$

where the h_{ill} is the point spread function (PSF) for illumination and h_{det} is the PSF for detection. The h_{ill} takes the same form as the expression for $|\mathbf{E}|^2$, which is given by

$$h_{ill} = |\mathbf{E}|^2 = |I_0|^2 + 4|I_1|^2 \cos^2 \phi + |I_2|^2 + 2 \cos 2\phi \text{Re}(I_0 I_2^*), \quad (7)$$

for linearly polarized illumination light ($\lambda = 532$ nm). The expression for h_{det} is given by

$$h_{det} = |I_0|^2 + 2|I_1|^2 + |I_2|^2, \quad (8)$$

for randomly polarized fluorescent light ($\lambda = 600$ nm). The contour plot of the point spread function H_{1p} for STIRFM is shown in Fig. 2. One can notice that the focus-splitting effect that is previously present in the contour plot of h_{ill} (Fig. 1d) disappears.

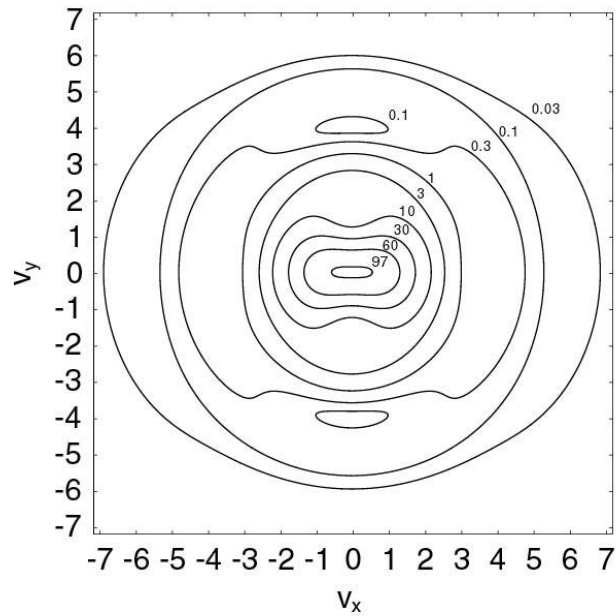


FIGURE 2: A contour plot of effective PSF (H) of the STIRFM ($\epsilon=0.6$) for one-photon illumination. The incident polarization is in parallel with x -axis. The numerical aperture is assumed to be 1.65.

However, for the two-photon excitation, the pinhole is removed since optical sectioning is intrinsic with two-photon excitation. As a result, the two-photon point spread function is

$$H_{2p} = h_{ill}^2. \quad (9)$$

For linearly polarized illumination light ($\lambda = 800$ nm), the contour plot of the two-photon point spread function H_{2p} is shown in Fig. 3. One can notice that the focus-splitting effect is more discernible because the intensity is squared.

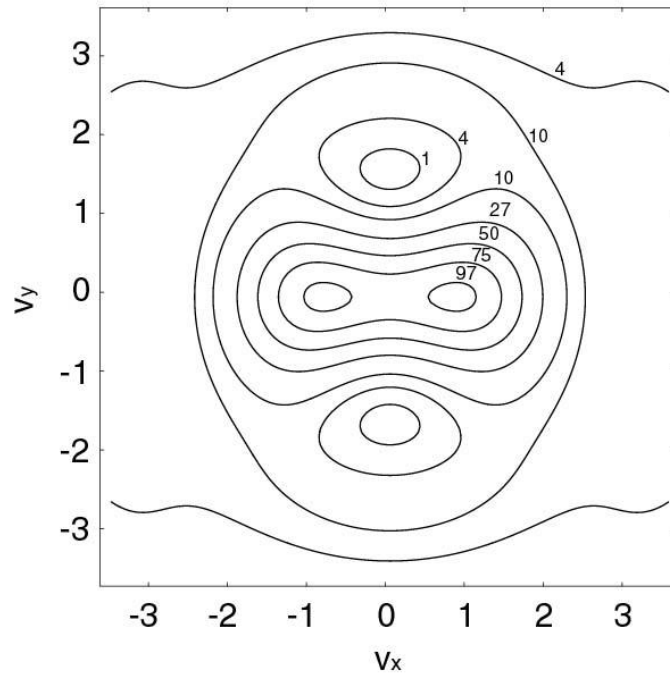


FIGURE 3: A density plot of effective PSF of the STIRFM ($\epsilon=0.6$) under two-photon excitation. The incident polarization is in parallel with x -axis. The numerical aperture is assumed to be 1.65.

In general, image formation in STIRFM is given by the convolution of the fluorescence intensity of a sample with the point spread function of the system. The fluorescence intensity function of a single quantum system such as a CdSe nanocrystal can be assumed to be a dirac-delta function, because its size (~ 6 nm) is much smaller than the Airy function of the focus ($0.5 \mu\text{m}$ in full-width half-maximum). Therefore the image of an NC can be approximately used as the effective PSF for STIRFM. However, it should be pointed that aggregates of the quantum dots would result a strong convolution between the H and the fluorescence intensity distribution of quantum dots. As a result, the focus-splitting effect would be more difficult to detect.

3. EXPERIMENTAL

The experimental configuration of STIRFM is shown in Fig. 4. We used a 532 nm diode-pumped cw laser (Spectra-Physics, Millennia IIs) as a one-photon excitation light source, and Titanium:Sapphire ultrashort pulsed laser (Spectra-Physics Tsunami) operating at wavelength 800 nm as a two-photon light source. The laser beam was expanded and focused at the glass-air interface by an objective (NA=1.65, Olympus). A central obstruction disk was inserted just prior to the reflection at the dichroic beamsplitter, producing a ring-beam illumination. An evanescent field was produced at the focus by obstructing all the beams with a convergence angle smaller than the critical angle of incidence. Fluorescence produced from the focus was then collected by the same objective, and re-focused at a photomultiplier tube (Oriel PMT, model 70680) to detect its intensity. For one-photon imaging, a 20 μm diameter pinhole was placed in front of the PMT to reduce the background scattered light. For collecting the fluorescence intensity, the sample was scanned in x and y -directions by a scanning stage (Physik Instrumente, Model P-517.3CL) to build up a two-dimensional fluorescence image. A special coverslip glass and immersion oil for the NA 1.65 objective had refractive index of 1.78. The high refractive index of the immersion oil and the coverslip glass increases the portion of the objective exit pupil in producing an evanescent field.

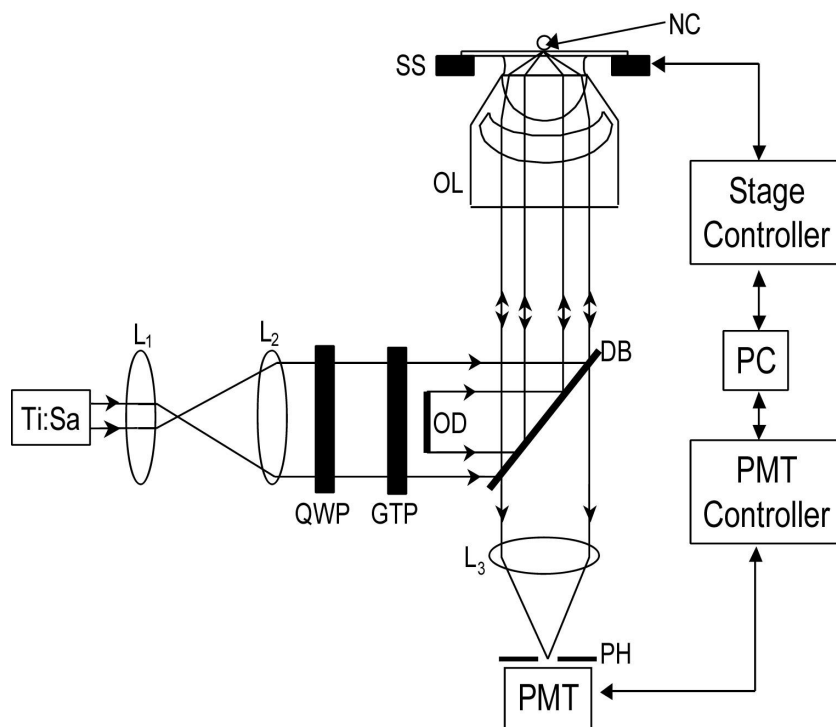


FIGURE 4: Experimental setup. Ring-beam illumination is produced by centrally obstructing the circular beam with an opaque disk just before the dichroic beam-splitter. QWP: $\lambda/4$ wave plate; GTP: Glan-Thompson Polarizer; OD: obstruction disk; SS: scanning stage; DB: dichroic beamsplitter; NC: nanocrystals, OL: objective lens (NA=1.65).

To probe the nonlinear absorption at the evanescent focus and the focal spot shape, CdSe quantum dot nanocrystals capped with trioctylphosphine oxide and trioctylphosphine (TOPO-TOP) were used as the fluorescence sample. The method of the nanocrystal preparation has been published elsewhere [14]. The mean diameter of the nanocrystals was ~ 6 nm and the peak fluorescence wavelength was at 600 nm. The nanocrystals were diluted in chloroform and a small droplet of the solution was dried onto a cleaned special coverslip glass. The average density of the quantum dots on the coverslip was 1 quantum dot per $1 \mu\text{m}^2$. The images of CdSe quantum dots in STIRFM under one-photon and two-photon excitation are shown in Fig. 5. In the two-photon imaging, the dependence of the NCs fluorescence on the laser input power is approximately quadratic (gradient of 2.0039 in the log-log plot), confirming the two-photon absorption by NCs. Note the definite split focal spot in the two-photon image of NCs. The direction of the split focus is along the direction of the incident polarization. In one-photon image, such focus-splitting effect is not observed, only the slight elongation towards the polarization direction can be noticed. This is expected from the theoretical simulation in the previous section, and is due to the pinhole placement at the detection path. The existence of the evanescent split focus is a direct observation of the depolarization effect of the high numerical aperture objective. Such depolarization at the focus enhances the longitudinal polarization component at the focus and thus can be used as a three-dimensional polarization excitation source. The size of the fluorescence intensity spots in one-photon image is approximately $0.4 \sim 0.6 \mu\text{m}$ and varies from place to place. However in the two-photon images, the individual peak of the split focus shows full-width half-maximum (FWHM) of ~ 100 nm, in the direction perpendicular to the incident polarization. This level of transverse resolution will proved to be useful in imaging single quantum systems.

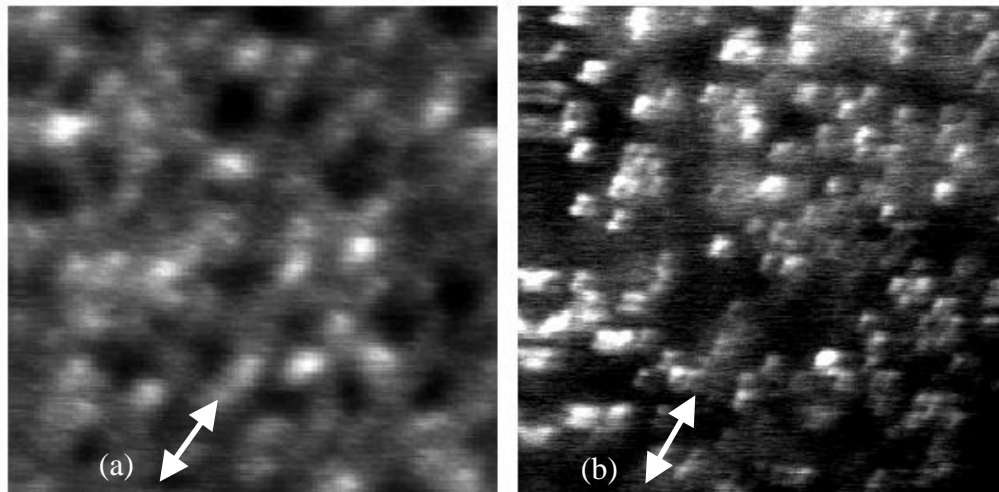


FIGURE 5: Fluorescence images of CdSe quantum dot nanocrystals on a coverslip glass ($10\mu\text{m} \times 10\mu\text{m}$) under (a) one-photon (532 nm) and (b) two-photon (800 nm) excitation. Polarization directions are indicated by the arrows.

4. CONCLUSIONS

In this paper, the nonlinear optical imaging process of scanning total internal reflection fluorescence microscopy is studied. The focused evanescent field in STIRFM can confine the excitation in a very small volume, hence effectively inducing the two-photon absorption. A rigorous theoretical investigation of the structure of the electric field near the focus produced by STIRFM has shown the focus-splitting due to depolarization. An appropriate PSF

analysis of the system has been provided for the interpretation of the quantum dot images and the focus-splitting effect. Both one-photon and two-photon images of CdSe quantum dot nanocrystals have been presented, and showed that due to the depolarization effect at the focus of high numerical-aperture objective, the focus can split into two peaks. Such split focus is only observed for two-photon images of nanocrystals. In one-photon case the presence of pinhole in the detection path effectively bars from observing the split focus.

It is expected that STIRFM will play an important role in the area of single molecular detection, three-dimensional polarization microscopy, fluorescence lifetime imaging, as well as the near-field applications such as near-field trapping, and near-field fabrication.

ACKNOWLEDGEMENTS

The authors are thankful to Dr. Xiaosong Gan for interesting discussions on applications, Associate Professor Paul Mulvaney and Mr. Craig Bullen of School of Chemistry, The University of Melbourne for CdSe quantum dot samples. The authors also acknowledge the support from the Australian Research Council.

REFERENCES

1. H. Watarai and F. Funaki, "Total internal reflection fluorescence measurements of protonation equilibria of rhodamine B and octadecylrhodamine B at a toluene/water interface", *Langmuir* 12, (1996) 6717.
2. M. Toriumi and M. Yanagimachi, "Time-resolved total-internal-reflection fluorescence spectroscopy and its applications to solid/polymer interface layers", *Microchemistry, Spectroscopy and Chemistry in Small Domains*, Masuhara H. et al., eds., Elsevier Science B.V., 257 (1994).
3. K. Stock, R. Sailer, W. S. L. Strauss, R. Pavesi, M. Lyttek, H. Emmert, and H. Schneckenburger, "Total internal reflection fluorescence spectroscopy and microscopy (TIRFS/TIRFM) in cell biology and photobiology", *Fluorescence Microscopy and Fluorescent Probes*, 3, (1999) 67.
4. R. Sailer, K. Stock, W. S. L. Strauss, M. Lyttek, and H. Schneckenburger, "Total internal reflection fluorescence microscopy (TIRFM) of acridine orange in single cells", *Endocytobiosis & Cell Res.*, 14, (2001) 129.
5. W. P. Ambrose, P. M. Goodwin, and J. P. Nolan, "Single-molecule detection with total internal reflection excitation: Comparing signal-to-background and total signals in different geometries", *Cytometry*, 36 (1999) 224.
6. M. F. Paige, E. J. Bjerneld and W. E. Moerner, "A comparison of through-the-objective total internal reflection microscopy and epi-fluorescence microscopy for single-molecule fluorescence imaging", *Single Mol.*, 2 (2001) 191.
7. M. Tokunaga, K. Kitamura, K. Saito, A. H. Iwane, and T. Yanagida, "Single molecule imaging of fluorophores and enzymatic reactions achieved by objective-type total internal reflection fluorescence microscopy", *Biochem. Biophys. Res. Commun.*, 235 (1997) 47.
8. T. Funatsu, Y. Harada, M. Tokunaga, K. Saito, T. Yanagida, "Imaging of single fluorescent molecules and individual ATP turnovers by single myosin molecules in aqueous solution", *Nature*, 374 (1995) 555.

9. R. D. Vale, T. Funatsu, D. W. Pierce, L. Romberg, Y. Harada, and T. Yanagida, "Direct observation of single kinesin molecules moving along microtubules", *Nature*, 380 (1996) 451.
10. T. Wazawa, Y. Ishii, T. Funatsu, and T. Yanagida, "Spectral fluctuation of a single fluophore conjugated to a protein molecule", *Biophys. J.*, 78 (2000) 1561.
11. Y. Sako, S. Minoghchi, and T. Yanagida, "Single-molecule imaging of EGFR signaling on the surface of living cells", *Nature Cell Biol.*, 2 (2000) 168.
12. R. M. Dickson, D. J. Norris, Y. L. Tzeng, and W. E. Moerner, "Three-dimensional imaging of single molecules solvated in pores of poly(acrylamide) gels", *Science*, 274 (1996) 966.
13. J. W. M. Chon, X. Gan, and M. Gu, "Splitting of the focal spot of a high numerical-aperture objective in free space", *Appl. Phys. Lett.*, 81, 1576 (2002).
14. C. B. Murray, D. J. Norris, and M. G. Bawendi, "Synthesis and characterization of nearly monodisperse CdE (E=S, Se, Te) semiconductor nanocrystallites", *J. Am. Chem. Soc.*, 115 (1993) 8706.
15. M. Born and E. Wolf, "Principles of Optics" Pergamon, New York, 1980.
16. M. Gu, "Advanced Optical Imaging Theory", Heidelberg, Springer, 1999.
17. M. Gu, "Principles of three-dimensional imaging in confocal microscopy", World Scientific, Singapore, 1996.
18. J. Tominaga, T. Nakano and N. Atoda, "An approach of recording and readout beyond diffraction limit with an Sb film", *Appl. Phys. Lett.*, 73, 2078 (1998).